

# Suppression of geometric induced artifacts in piezoresponse force microscopy of III-N semiconductor nanowires

L. Jaloustre<sup>1,2</sup>, S. Le-Denmat<sup>1</sup>, T. Auzelle<sup>3</sup>, M. Azadmand<sup>3,4</sup>, L. Geelhaar<sup>3</sup>, F. Dahlem<sup>2</sup>, and R. Songmuang<sup>1</sup>

<sup>1</sup>Univ. Grenoble Alpes, CNRS, Grenoble INP, Institut Néel, 38000 Grenoble, France

<sup>2</sup>LTDS, Ecole Central de Lyon, France

<sup>3</sup>Paul-Drude-Institut für Festkörperelektronik, Leibniz-Institut im Forschungsverbund Berlin e.V., Hausvogteiplatz 5-7, 10117 Berlin, Germany

<sup>4</sup>L-NESS and Dipartimento di Scienza dei Materiali, Università di Milano – Bicocca, Milano, Italy

This work presents systematic investigations of piezoresponse force microscopy (PFM) on III-N semiconductors. In bulks and thin films, the electrostatic artifacts in the PFM signal were minimized by using a stiff cantilever and a top metallic electrode. Depending on the electrode geometry, the clamping and bending effects can concurrently occur. While the clamping effect only decreases the piezoresponse amplitude, the bending one can either increase or decrease the amplitude and; if it is dominant, the phase signal becomes rotating by 180°. The reduced lateral dimension of the nanowires can suppress both artifacts by homogenizing the field distribution. The phase of the piezoresponse from GaN, Al<sub>0.9</sub>Ga<sub>0.1</sub>N/GaN, and AlN nanowires is always coherent with their polarity, and the extracted  $d_{33}$  values agree with their respective bulk ones. We suggest that the nanowire is a relevant geometry to perform quasi-quantitative PFM, and there is no giant piezoelectric in this type of nanowires as claimed in the literature.

After the publications of ZnO nanowire-nanogenerators and self-powered nano-systems [1-2], piezoelectric semiconductor nanowires such as ZnO and GaN have gained rising attention for mechanical energy scavenging using piezoelectric effect. Higher energy conversion efficiency was further expected since a giant piezoelectric effect was extracted from 60 nm-diameter GaN nanowires by using vector piezoresponse force microscopy (PFM) measurements [3-4]. In PFM, a conductive tip is used as a movable top electrode to apply an alternated electric field and detect associated displacement caused by the inverse piezoelectric effect, simultaneously. Nevertheless, it remains challenging to obtain quantitative PFM analyses and to understand the PFM signal; particularly, from piezoelectric semiconductors because of their low piezoelectric coefficient values (2-6 pm/V). Besides, various measurement parameters could influence on the PFM response such as electrostatic effects [5], nanoscale SFM tip diameter [6], substrate bending [7], substrate clamping [8], signal amplification by mechanical resonance of cantilever [9], cantilever buckling [9], topographic variation, etc. Those parameters introduce artifacts to the PFM signal, thus providing incorrect piezoelectric coefficients and material polarity. Possibly, the mentioned artifacts might be the reasons for the inconsistent interpretations of the PFM signal from III-N thin films from different groups [10,11,12,13,14]. This issue should be clarified because PFM is one of the general tools used for identifying the mixture of crystal polarities and piezoelectric properties of nitrides [15,16,17,18,19]. Without clarifying this inconsistency, the giant piezoelectricity in GaN nanowires and nanobelts remains questionable as it might result from the measurement artifacts.

In this paper, we performed systematic PFM studies on III-N in various forms. The electrostatic coupling, the clamping, and the substrate bending effects usually mislead the PFM signal interpretation from bulk and thin films. Nanowires compared to bulk or thin-film are shown as a relevant geometry to avoid geometric induced artifacts in PFM signal, thus allowing correct determinations of the piezo-coefficients and polarity of materials. Our experimental results are supported by two-dimensional finite element simulations via COMSOL software. It was found that there is no giant piezoelectricity in GaN nanowires as claimed in literature [3, 4, 20, 21, 22].

Wurtzite III-Nitride is a non-centrosymmetric crystal, which possesses both spontaneous and piezoelectric polarization. The spontaneous one originates from the non-ideality of the crystal

structure, while the piezoelectric one is caused by the displacement of the center of gravity of cations and that of anions under external stress. The compressive stress along the  $c$ -axis of Ga-GaN or the [0001] direction, moves the Ga atoms closer to the nitrogen basal atoms, leading to a *negative* piezoelectric polarization in this direction. The orientation of the piezoelectric polarization of III-Nitrides is similar to that of II-VI such as ZnO, but it is opposite to the ones of other III-V compounds [23]. Reversely, the applied electric field also introduces an ionic displacement in the crystal, resulting in a lattice deformation. If the electric field is applied along the  $c$ -axis, the anions (cations) would displace in the opposite (same) direction to that of the applied field [24]. In the case of III-N, the deformation preferentially occurs through the distortion of the tetrahedral angle rather than the modification of tetrahedral distance.

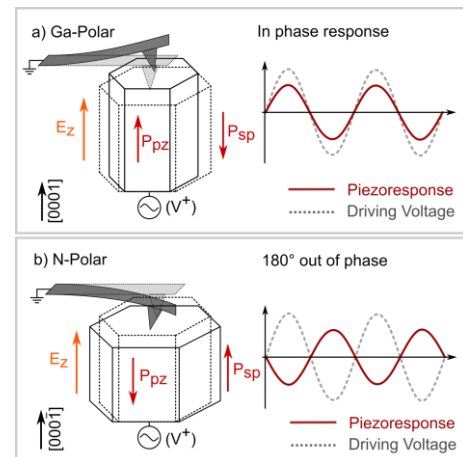


FIG. 1 Schematic illustration presents the piezoresponse from (a) Ga-GaN and (b) N-GaN, under the applied  $V_{AC}$  at the substrate backside. The opposite direction of spontaneous polarization and piezoelectric polarization in GaN is shown.

Figure 1 schematically describes the expected piezoresponse from Ga- and N-polar GaN bulk substrates in the sample bias configuration. When a positive voltage is applied at the backside of the sample, a positive field would appear along the [0001] direction. Using the Voigt notation, the strain along the  $c$ -axis ( $\epsilon_{33}$ ) of Ga-GaN under the applied field ( $E_3$ ) parallel to the [0001] direction is given by  $\epsilon_{33}=d_{33}E_3$ . The  $d_{33}$  is the piezoelectric coefficient defined with respect to the [0001] axis, which is

positive in III-N [25]. The crystal expands, or the  $\epsilon_{33}$  is positive when the positive  $E_3$  is applied [The left panel of Figure 1(a)], while the  $\epsilon_{33}$  is negative or the crystal contracts when the electric field direction is reversed. The phase difference between the PFM signal and the applied  $V_{AC}$  at the substrate is  $0^\circ$  for Ga- GaN [The right panel of Figure 1(a)], while the one of N-GaN shifts to  $180^\circ$  [Figures 1(b)]. This PFM phase response; if it is measured correctly, it can be used as a non-destructive method to determine the material polarity.

In 2002, Rodriguez *et al.* performed a polarity imaging on a one- $\mu\text{m}$  thick GaN layer on a sapphire substrate, by monitoring its PFM phase signal [10-11]. These authors [10-11] and Stoica *et al.* [12] explained the observed phase signal by using a total polarization, which is dominated by spontaneous polarization. However, the direction of spontaneous and piezoelectric polarization in III-Nitrides are *opposite* [23] as seen in Figure 1. Thus, their PFM phase description *indicates the  $180^\circ$  phase offset*. Moreover, the sign of the applied electric field (differing from the voltage) which depends on the bias configuration, should be carefully defined; otherwise, the phase signal can be  $180^\circ$  shifted, as well.

In 2011, Brubaker *et al.* noticed that the PFM phase response from a 100-nm AlN layer on Si(111) agrees with the piezoelectric polarization [13-14], unlike those of GaN reported in ref [11-13]. In 2015, Minj *et al.*, used the PFM phase to locate Ga- and N-polar regions in single nanowires [26], following Rodriguez *et al.* [10-11]. For equivalent ZnO material, Scrymgeour *et al.* showed the consistent PFM phase signal of ZnO bulk with the piezoelectric polarization [27], while that of ZnO thin films measured by Guillemain *et al.* [28], was implicitly coherent with the spontaneous one. None of those authors; except Brubaker *et al.*, has pointed out these PFM phase discrepancies in the literature.

Here we explore the PFM measurements on different types of III-N semiconductors. The samples under investigations were bulk Ga- and N-GaN substrates with a thickness of 400  $\mu\text{m}$  from LumiLog. Ga-GaN and N-GaN layers with a thickness of 500-nm on 200 nm-AlN buffer layer, as well as a 200-nm Al-AlN layer on highly doped Si(111) substrates from Kyma technology, were also measured. On each sample, 5-10 nm Ti/20nm Au circular top electrodes with a diameter ranging from 250 to 1000  $\mu\text{m}$  were deposited. A non-piezoelectric 250-nm  $\text{SiO}_2$  layer on a highly doped Si substrate and a commercial PZT bulk PCI300 from PI Ceramics with a known polarization direction were used as reference samples.

The nanowire samples were grown by using plasma-assisted molecular beam epitaxy. The undoped GaN and undoped  $\text{Al}_{0.9}\text{Ga}_{0.1}\text{N}$ /GaN nanowires were deposited on highly n-doped Si(111) substrates [29, 30], while the AlN nanowires were grown on sapphires covered by conductive TiN layer obtained by sputtering [31]. The carrier concentration of undoped GaN nanowires was in the range of  $10^{17} \text{ cm}^{-3}$  [32]. The polarity of GaN nanowires is N-polar, proven by KOH chemical etching [33], and deduced by high-resolution scanning transmission electron microscopy (HR-STEM) analyses of the equivalent nanowires [34]. The AlN nanowires are suggested to have Al-polarity [31]. The nanowire details are summarized in Table I.

Table I: Detail of the nanowires studied in this work. The samples are undoped.

	GaN		AlGaIn/GaN	AlN
Length (nm)	550	1000	180/600	800
Diameter (nm)	30-50	30-50	60	80
Polarity	N-Polar [46]			Al-Polar [43]
Carrier conc. ( $\text{cm}^{-3}$ )	$10^{17}$		Insulating/ $10^{17}$	Insulating

To fabricate a top electrode on undoped GaN nanowire ensemble with the length of 1000 nm, the nanowires were embedded inside Polymethyl Methacrylate (PMMA). Then,  $\text{O}_2$

plasma etching was applied to remove the PMMA layer that covered on the top of nanowires. Afterward, the circular 10-nm Ti/ 60-nm Pt top electrode with a diameter of 1000  $\mu\text{m}$  was deposited. All the samples were glued on a metallic holder by silver epoxy or silver paste which also act as a back electrode.

The PFM measurements were performed by using Bruker D3100-SFM, with an external AC and DC excitation and a lock-in detection via a Zurich instrument HF2LI. The resolution limit of our setup is  $\sim 0.5 \text{ pm}$ . The conductive SFM tip is coated by Ti/Ir or Pt/Ir with a spring constant of 0.2, 3 and 40 N/m. The bias was applied at the backside of the substrates, while the SFM tip and the top electrode were electrically connected to ground. The frequency dependence of the PFM signal was measured to ensure that there is no mechanical amplification at 17 kHz which was the selected frequency for PFM measurements. A non-local electrostatic contribution was determined via a contact potential difference ( $V_{CPD}$ ) by an open-loop Kelvin Probe Force Microscopy (KPFM) in a standard intermittent mode [35].

It is known that the background can contribute to the PFM signal; therefore, all our analyzed piezoresponse amplitude was extracted from the X-signal rather than the R-signal of the lock-in amplifier output [36]. In any case, we verified that the Y-signal is nearly zero, allowing the determination of the PFM phase by the sign of the X-value. A negative sign is out-of-phase in respect to the excitation voltage, while a positive one is in-phase. The effective piezoelectric constants ( $d_{33}$ ) were extracted from the slope of the X-signal versus the applied  $V_{AC}$  amplitude.

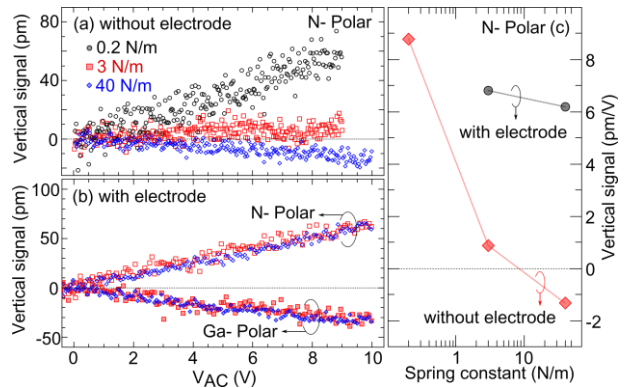


FIG. 2 The vertical PFM signal versus the applied  $V_{AC}$  from (a) N-GaN bulk without a top electrode, (b) N- and Ga-GaN bulk, at the center of a top electrode with a diameter of 500  $\mu\text{m}$ . These values were measured by using the SFM cantilever stiffness of 0.2 N/m ( $\circ$ ), 3 N/m ( $\square$ ) and 40 N/m ( $\blacklozenge$ ). (c) The effective  $d_{33}$  values as extracted from the PFM signal of N-GaN bulk with and without top electrodes, plotted as a function of the spring constants .

Figure 2 presents the investigations of the electrostatic effect on the PFM response of GaN. The concurrent electrostatic force often occurs between the SFM tip/cantilever and the sample surface because of the surface potential and surface charges [37]. This force can either attract or repulse the SFM cantilever, which modifies the cantilever motion caused by the crystal displacement and changes the phase and amplitude of the piezoresponse. This electrostatic contribution has the same frequency as the excitation voltage; thus, it cannot be filtered out via lock-in techniques. Nevertheless, such an effect can be minimized by using a high spring constant SFM cantilever, which is less sensitive to the electrostatic force, or it can be compensated by applying  $V_{DC} = V_{CPD}$  during PFM measurements [38]. Another possibility is to equalize the potential between the SFM tip/cantilever and the sample surface, by depositing the metal electrode on the sample surface and electrically connecting it to the SFM cantilever [5]. Figure 2(a) summarizes the vertical PFM signal as a function of the applied  $V_{AC}$  from the N-GaN bulk

without top electrode. The measurements were performed by using the SFM cantilevers with different spring constants, i.e., 0.2 N/m, 3 N/m, and 40 N/m. In the case of the cantilevers of 0.2 and 3 N/m, the in-phase vertical signal with the slope or the effective  $d_{33}$  of  $\sim 8$  pm/V and  $\sim 1$  pm/V; respectively, was found. The phase signal became out-of-phase or was reversed by  $180^\circ$  with the extracted  $d_{33}$  of  $\sim 1.2$  pm/V, once the 40 N/m cantilever was used. In the latter case, the phase signal agrees with the piezoelectric polarization direction of N-GaN as described in Figure 1(b). The in-phase PFM signal obtained by 0.2 and 3 N/m cantilevers indicates that this response is dominated by the electrostatic contribution, which is in-phase with the electrical excitation. In this particular case, the electrostatic force counteracts the cantilever motion induced by the crystal displacement. However, it is not straightforward to compensate this force by applying  $V_{DC}=V_{CPD}$  as suggested by ref [38] during the PFM measurements on semiconductors because this value depends on the surface band bending [37], which can be varied by the applied  $V_{AC}$ . The fixed value of the applied  $V_{DC}$  might not be sufficient to cancel the electrostatic potential.

The extracted  $d_{33}$  value from the N-polar GaN without top electrode using 40 N/m cantilever (1.2 pm/V) in Figure 2 (a) is less than the expected value of 2.3 pm/V of GaN [25]. Using a conductive SFM tip as a top electrode is a standard PFM configuration that offers a high lateral resolution. However, it also localizes the applied field in a small volume underneath the tip, which can reach  $10^9$  V/m, depending on the tip radius, the dielectric constant, and the sample thickness [39]. This highly focused field results in a clamping effect; that is, the unexcited surrounding material, including the inactive Si substrate restricts the mechanical deformation in the excited volume [17]. Besides, if there is a non-piezoelectric oxide covering the surface of piezoelectric material, the majority of the field might localize in that layer. Both effects result in a lower PFM amplitude.

Another way to suppress the electrostatic contribution is to use the metallic top electrode which is electrically connected to the SFM cantilever [5]. Figure 2(b) shows the PFM measurements performed at the center of the 500- $\mu$ m diameter top electrode on Ga- and N-GaN bulk, using the 3 and 40 N/m cantilever. The electrode center is a symmetric point, where the in-plane displacement does not contribute to the vertical motion of the cantilever [40]. Thus, the vertical signal directly corresponds to the mechanical motion of the crystal surface. In other words, at this position, there is no buckling effect of the cantilever, which modifies the PFM amplitude and phase.

As revealed by Figure 2(b), there is no significant difference between the PFM responses obtained by using two different cantilever stiffness, reflecting the electrostatic screening by the electrode. However, the phase signal from these two samples was reversed by  $180^\circ$ , in comparison to those from the ones without the top electrode. For examples, the out-of-phase signal from N-GaN bulk became in-phase, while Ga-GaN bulk showed an out-of-phase signal when the PFM was measured at the electrode center. Figure 2(c) summarizes the effective  $d_{33}$  extracted from the PFM signal of N-GaN bulk, without and with top electrodes, as a function of cantilever stiffness.

Although the  $180^\circ$  phase difference between Ga- and N-GaN bulks indicates that the PFM signal is related to the material polarity, it cannot be directly described by a simple piezoelectric displacement of the sample surface, especially for the large  $d_{33}$  up to 6 pm/V from N-polar GaN bulk. This  $180^\circ$  phase offset

cannot be attributed to the electrostatic force because it was entirely suppressed by the top electrode and by the high stiffness cantilever as confirmed by KPFM measurements.

The summary of the extracted  $d_{33}$  as a function of the top electrode diameter is presented in Figure 3. These values were taken at the center of the electrode of Ga- and N-GaN bulk and thin films on Si(111), as well as a 200 nm Al-AlN on Si(111). The absolute value of these  $d_{33}$  systematically decreases in a smaller contact size, due to the clamping effect. Importantly, the  $d_{33}$  of nearly all samples changed to the opposite sign when the SFM tip was used for applying the bias, instead of using the top electrode. In the case of N-GaN thin film, the signal reached the resolution limit; thus, the sign could not be identified. This sign inversion shown in Figure 3 might be an indication for the bending motion of the substrate, which can reverse the piezoresponse by  $180^\circ$  once it is dominant [7].

To qualitatively understand the crystal displacement behavior detected by PFM, we performed two-dimensional finite element simulations of piezoelectric displacements of Ga-GaN bulk by using COMSOL. The simulated thickness and width are 400  $\mu$ m and 6 mm, respectively, which is equivalent to the size of the samples in our experiments. The top electrode diameter was varied from 100 nm to 5 mm, while the substrate backside was entirely covered with a metallic electrode. The effect of free carriers in semiconductor and the bandstructure were not considered. One-volt bias was applied at the substrate backside, while the top electrode was grounded.

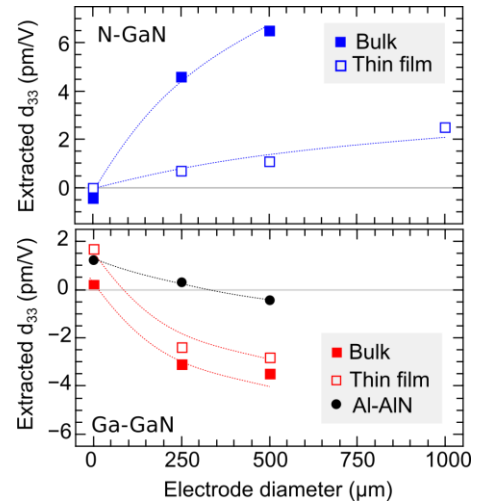


FIG. 3 The  $d_{33}$  value extracted from the vertical signal plotted as a function of the top electrode diameter from Ga- and N-GaN bulk and thin films, as well as Al-AlN on Si(111). The PFM measurements were performed at the electrode center. The dashed lines are the guide for the eyes.

Figures 4(a)-(b) are the contour plots showing the vertical displacement in the [0001] or the  $z$ -direction of Ga-GaN bulk with the 500- $\mu$ m top electrode, simulated by using unclamped and clamped boundary conditions of the substrate backside, respectively. These results reveal that the substrate bending can occur in the former configuration, leading to the vertical displacement of the top crystal surface below the electrode opposite to that of the clamped one. The sectional profiles of the vertical displacement from the unclamped Ga-GaN bulk with the top electrode diameter of 1- $\mu$ m and 500- $\mu$ m are plotted in comparison in Figures 4(c)-(d). The black solid line presents the vertical displacement of the top surface while the red line is that of the bottom one. The evolution of the vertical displacements taken at the electrode center is plotted as a function of the top electrode diameter in Figure 4(f).

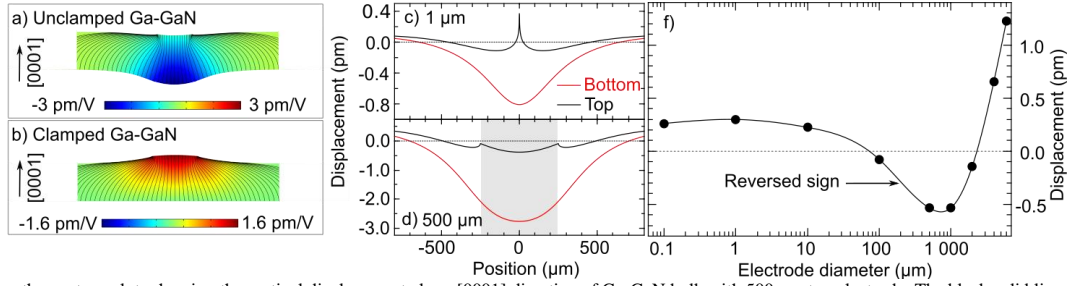


FIG. 4 (a)-(b) are the contour plots showing the vertical displacement along [0001] direction of Ga-GaN bulk with 500  $\mu\text{m}$  top electrode. The black solid lines present the line field distribution. (c)-(d) Sectional profiles of the vertical displacement along the  $c$ -axis at the top (black line) and bottom surface (red line) of an unclamped Ga-GaN bulk with a top electrode diameter of 1  $\mu\text{m}$  and 500  $\mu\text{m}$ , respectively. The substrate backside was biased at 1 V. The grey shade defines the area below the top electrode. (f) Summary of the vertical displacement taken at the electrode center as a function of the electrode diameter.

For the electrode diameter less than 100  $\mu\text{m}$  in this particular geometry, the positive displacement corresponds to the piezoelectric polarization direction as expected for Ga-GaN bulk with a positive backside bias. The lower displacement than the bulk value is attributed to the restricted crystal motion caused by an unexcited surrounding crystal or the clamping effect. In this particular geometry, the simulations show that the sign of the displacement becomes negative when the electrode diameter is higher than 100  $\mu\text{m}$ , and it turns positive again once the electrode diameter is above 2 mm. The inversion of the PFM sign to a negative value results from the dominant bending of the unclamped substrate because of an asymmetric field distribution along  $z$ -direction as shown in Figure 4(a).

As the substrate bending originates from the piezoelectric effect, its sign also depends on the material polarity. The bending displacement is superimposed with the piezoelectric induced thickness variation, with an opposite sign. If the bending contribution is dominant, the  $180^\circ$  offset would appear in the vertical PFM signal. When the top and bottom electrodes entirely cover the substrate surface, the clamping and bending effects are both suppressed because the applied field becomes symmetric and uniformly distributes over the substrate. Therefore, the detected piezoresponse from the top surface could approach theoretical value. For a fully clamped substrate, the simulations suggest that the vertical displacement at the electrode center is always positive and increases with the electrode size as a result of the reduced clamping effect. To summarize, the bending effect is caused by an asymmetric field distribution due to an asymmetry between the top and bottom electrodes. The clamping effect is induced by the localized field caused by a small contact size in comparison to the sample dimension. The similar tendency was found in GaN thin film on Si.

The simulated results support our interpretations that the bending is responsible for the  $180^\circ$  phase inversion found in Figure 3. Possibly, a perfect clamping backside substrate was *not* reached by a standard way of gluing the samples, resulting in a substrate bending. When the contact size is less than a critical value, the bending displacement can be minimized, but the clamping effect becomes superior. The situation depends on various parameters such as the substrate and contact geometry, the mechanical characteristics, the gluing material, as well as the sample holder [16,41,42]. It was found in other measurement techniques which can access only the displacement at the top surface, for examples, single interferometer [16,43], and laser Doppler vibrometer [44,45]. Besides these simulations, our vector PFM measurements, which simultaneously detect the lateral and vertical displacements also indicated that the sign inversion of the vertical PFM signal was due to the substrate bending [40].

The degree of bending and clamping effects should decrease in high-aspect-ratio structures; for examples, nanowires or nanocolumns because of the improvement of the field homogeneity and symmetry. Here, the PFM measurements were

performed on III-N nanowires such as GaN,  $\text{Al}_{0.9}\text{Ga}_{0.1}\text{N}/\text{GaN}$ , and AlN, with the aspect ratio of around 1:10. Figures 5(a)-(b) show the side view SEM image and the top view topography acquired by SFM in intermittent (tapping) mode of typical undoped GaN nanowire ensemble. The piezoresponse was investigated on the top of these nanowires.

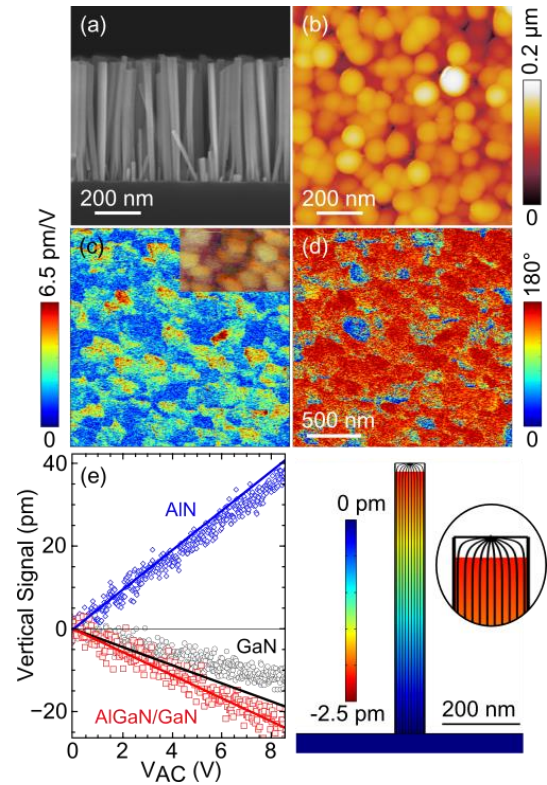


FIG. 5 (a) Side view SEM image and (b) top view topography by SFM intermittent mode of typical GaN nanowire ensemble. (c)-(d)  $2 \times 2 \mu\text{m}^2$  PFM amplitude and phase of N-polar GaN nanowires with  $V_{AC}=6 \text{ V}$  [46]. The inset shows the corresponding nanowire topography simultaneously acquired during the PFM measurement. (e) The vertical signal plotted as a function of the applied  $V_{AC}$  from GaN, AlN, and AlGaIn/GaN nanowires. The solid lines present the vertical displacement versus the applied voltage of each material obtained by COMSOL simulation. The right panel shows a contour plot of the vertical displacement of an N-polar GaN nanowire on Si substrate under the application of 1 V on Si while the top of the nanowire is grounded. The black solid lines represent the field distribution inside the nanowire.

Figures 5(c)-(d) present a  $2 \times 2 \mu\text{m}^2$  scanning PFM amplitude and phase signal from N polar-GaN nanowires by applying  $V_{AC}=6 \text{ V}$  on Si substrate and using 3 N/m cantilever. The inset shows the top view SFM image of the nanowire topography in a contact mode, simultaneously obtained during the PFM measurements. The PFM signal is highly visible in the nanowire regions. This signal is *out-of-phase* with respect to the electrical excitation in most wires, consistent with the piezoelectric

polarization direction of N-polar GaN. Figure 5(e) presents a typical PFM vertical signal versus an applied  $V_{AC}$ , from GaN,  $Al_{0.9}Ga_{0.1}N/GaN$ , and AlN nanowires, in comparison. The measurements were performed at different positions on the sample surface, using the 40 N/m cantilevers which are less sensitive to the electrostatic effect. The phase response from N-polar GaN and  $Al_{0.9}Ga_{0.1}N/GaN$  nanowires are always *out-of-phase*, confirming the phase signal shown in Figure 5(d). In contrast, the positive PFM signal from AlN nanowires corresponds to *in-phase response*, agreeing with the metal polarity of the investigated AlN nanowires observed by HR-STEM for one dispersed AlN nanowire from the same sample [31].

The extracted  $d_{33}$  from the GaN nanowires were in the range between 1-1.6 pm/V, while the higher values from the  $Al_{0.9}Ga_{0.1}N/GaN$  nanowires in the range of 2.4-3.6 pm/V were systematically found. The value of around 4.5 pm/V was obtained from AlN nanowires. The piezoresponse was also investigated in the long and thin GaN nanowire ensemble covered by a one-mm diameter metallic electrode. In this case, the electrostatic effect was screened entirely, confirmed by KPFM measurements. The phase response is similar to the one presented in Figure 5 (e) with the extracted  $d_{33}$  of 1.5-2 pm/V. This slightly higher  $d_{33}$  is explained by the improved electrical contact between the metallic electrode and the nanowires, together with an increasing contact area.

We performed COMSOL simulations of GaN and  $Al_{0.9}Ga_{0.1}N/GaN$  nanowires with N-polarity and AlN nanowires with Al-polarity on Si substrate, by setting a fully-clamp boundary condition at the backside of Si substrate. The structural parameters for the simulations are selected to be as close as possible to the investigated samples. The diameter and the length of GaN nanowire is 50 nm and 600 nm, respectively. For  $Al_{0.9}Ga_{0.1}N/GaN$  nanowires, the diameter of 50 nm is chosen, while the length of  $Al_{0.9}Ga_{0.1}N$  section is 200 nm and that of GaN stem is 600 nm. The simulated structure of AlN nanowires is 50 nm in diameter and 800 nm in length. The top electrode diameter is set at 1 nm, to imitate the contact area between the SFM tip diameter and the nanowire. The bottom surface of Si substrate is fully covered by the electrode. The solid lines in Figure 5(e) present the simulated vertical displacements of the nanowire top surface as a function of applied  $V_{AC}$ , which agree with the experimental results. The extracted  $d_{33}$  and the polarity from PFM measurements of the investigated nanowires are summarized in Table II, in comparison with the bulk values and the ones obtained from COMSOL, together with the expected polarity of each sample. This table shows that the phase response from the nanowires is consistent with the expected polarity of the

investigated nanowires. The large fluctuation and the deviations from the predicted  $d_{33}$  in the case of  $Al_{0.9}Ga_{0.1}N/GaN$  nanowires is possibly because of the chemical content variation among each  $Al_{0.9}Ga_{0.1}N/GaN$  nanowires. The lower  $d_{33}$  of GaN and AlN nanowires might be caused by the tip-surface contact characteristic or the effect of the free carriers in nanowires in the case of GaN, which must be further explored. In any case, the giant piezoelectric effect was not observed, in the nanowires which were grown by the same technique as the ones in ref [3-4].

Table II: Summary of the extracted  $d_{33}$  and the polarity from PFM measurements in comparison with the bulk values and the ones obtained from COMSOL, together with the expected polarity of each sample.

Nanowires	PFM		$d_{33}$ (pm/V)		Polarity
	$d_{33}$ (pm/V)	Polarity	Bulk	Nanowire (COMSOL)	
Undoped GaN	1-1.6	N	2.29 [25]		N [34]
Undoped GaN with top electrode	1.5-2	N	2.29 [25]	2.2*	N [34]
$Al_{0.9}Ga_{0.1}N/GaN$	2.4-3.6	N	3 [47]	2.8	N [34]
AlN	4.5	Al	5.35 [25]	4.85	Al [31]

\*Considering that the top surface is completely covered by metal, thus the diameter of the top electrode is 50 nm for the simulation.

In conclusion, we present the influences of the electrostatic contribution on the PFM signal from GaN bulk and thin films, as well as a possibility to suppress it, either by using the high stiffness cantilever or by using the top metallic electrode. However, the bending and clamping effects can play a role on the PFM phase and amplitude, depending on the electrode size and the sample geometry. We show that the  $180^\circ$  phase inversion in piezoresponse is likely coming from a non-ideal clamping boundary of the substrate backside, which introduces the bending displacement superimposing with the piezo-one. Both effects can be diminished in high aspect ratio structures. Our results suggest an alternative way to reach quasi-quantitative PFM by reducing the lateral dimension of the measured materials, together with the use of high stiffness cantilever. The polarity of III-N nanowires extracted from the PFM is consistent with the expectations, while the obtained  $d_{33}$  values agree with finite element simulations using bulk parameters. Thus, we suggest that the giant piezoelectric effect does not exist in GaN, AlN and AlGaN/GaN nanowires, which are equivalent to the ones in ref [3-4]. We also proposed that the interpreted Ga-polar area in GaN nanowires shown by Minj *et al.* in ref [26] is rather N-polar one.

The authors acknowledge the assistance from Nanofab/Néel Institute for sample fabrications. The work is financially supported by ARC-Energy project, NanoTribelec-ANR project, GaNEX, and the German Bundesministerium für Bildung und Forschung (Project No. FKZ: 13N13662).

<sup>1</sup> Z. L. Wang, J. Song, Science 312, 5771 (2006).

<sup>2</sup> X. Wang, J. Song, J. Lui, Z. L. Wang, Science 316, 5821 (2007).

<sup>3</sup> M. Minary-Jolandan, R. A. Bernal, and H. D. Espinosa, MRS Communications 1, 45(2011).

<sup>4</sup> M. Minary-Jolandan, R. A. Bernal, I. Kuljanishvili, V. Parpoil, and H. D. Espinosa, Nano Lett. 12, 970 (2012)

<sup>5</sup> J. A. Christman, R. R. Woolcott Jr., A. I. Kingon, and R. J. Nemanich, Appl. Phys. Lett. 73, 3851 (1998).

<sup>6</sup> T. Jungk, A. Hoffmann, and E. Soergel, Appl. Phys. A 86, 353 (2007).

<sup>7</sup> A. L. Kholkin, Ch. Wüthrich, D. V. Taylor, and N. Setter, Rev. Sci. Instrum. 67, 1935 (1996).

<sup>8</sup> K. Lefki and G. J. M. Dormans, J. Appl. Phys. 76, 1764 (1994).

<sup>9</sup> B. Voigtländer, Scanning Probe Microscopy: Atomic Force Microscopy and Scanning Tunneling Microscopy, Springer, Berlin, Heidelberg (2015).

<sup>10</sup> B. J. Rodriguez, A. Gruverman, A. I. Kingon, and R. J. Nemanich, and O. Ambacher, Appl. Phys. Lett. 80, 4166 (2002).

<sup>11</sup> B.J. Rodriguez, A. Gruverman, A.I. Kingon, and R.J. Nemanich, J. Cryst. Growth 246, 252 (2002).

<sup>12</sup> T. Stoica, R. Calarco, R. Meijers, and H. Lüth, Appl. Sur. Sci. 253, 4300 (2007).

<sup>13</sup> M. D. Brubaker, I. Levin, A. V. Davydov, D. M. Rourke, N. A. Sanford, V. M. Bright, and K. A. Bertness, J. Appl. Phys. 110, 053506 (2011).

<sup>14</sup> M. D. Brubaker, A. Roshko, P. T. Blanchard, T. E. Harvey, N. A. Sanford, and K. A. Bertness, Mater. Sci. Semicond. Process. 55, 67 (2016).

<sup>15</sup> M. Akiyama, T. Kamohara, N. Ueno, M. Sakamoto, K. Kano, A. Teshigahara, and N. Kawahara, Appl. Phys. Lett. 90, 151910 (2007).

<sup>16</sup> K. Tonisch, V. Cimalla, Ch. Foerster, D. Dontsov, and O. Ambacher, phys. stat. sol. (c) 3, 2274 (2006).

<sup>17</sup> T. Kamohara, M. Akiyama, and N. Kuwano, Appl. Phys. Lett. 92, 093506 (2008).

<sup>18</sup> E. Yarar, V. Hrkac, C. Zamponi, A. Piorra, L. Kienle, and E. Quandt, AIP Advances 6, 075115 (2016).

<sup>19</sup> S. Fichtner, N. Wolff, G. Krishnamurthy, A. Petrus, S. Bohse, F. Lofink, S. Chemnitz, H. Kohlstedt, L. Kienle, and B. Wagner, J. Appl. Phys. 122, 035301 (2017).

<sup>20</sup> M.-H. Zhao, Z.-L. Wang, and S. X. Mao, Nano Lett. 4, 587 (2004).

<sup>21</sup> N. Tiwary, R. Sarkar, V. R. Rao, and A. Laha, Joint IEEE International Symposium on the Applications of Ferroelectrics, European Conference on Application of Polar Dielectrics, and Piezoelectric Force Microscopy Workshop, (ISAF/ECAPD/PFM), 2016 DOI: 10.1109/ISAF.2016.7578091

<sup>22</sup> D. X. Wu, H. B. Cheng, X. J. Zheng, X. Y. Wang, D. Wang, J. Li, Chin. Phys. Lett. 32, 108102 (2015).

<sup>23</sup> F. Bernardini, V. Fiorentini, and D. Vanderbilt, Phys. Rev. B 56, R10024 (1997).

<sup>24</sup> T. Kamiya, Jpn. J. Appl. Phys. 35, 4421 (1996).

- <sup>25</sup> O. Ambacher, J. Majewski, C. Miskys, A. Link, M. Hermann, M. Eickhoff, M. Stutzmann, F. Bernardini, V. Fiorentini, V. Tilak, B. Schaff, and L. F. Eastman, *J. Phys. Condens. Matter.* 14, 3399 (2002).
- <sup>26</sup> A. Minj, A. Cros, N. Garro, J. Colchero, T. Auzelle, and B. Daudin, *Nano Lett.* 15, 6770 (2015).
- <sup>27</sup> D. A. Scrymgeour and J. W. P. Hsu, *Nano Lett.* 8, 2204 (2008).
- <sup>28</sup> S. Guillemin, R. Parize, J. Carabetta, V. Cantelli, D. Albertini, B. Gautier, G. Brémond, D. D. Fong, H. Renevier, and V. Consonni, *Nanotechnology* 28, 095704 (2017).
- <sup>29</sup> R. Songmuang, O. Landré, and B. Daudin, *Appl. Phys. Lett.* 91, 251902 (2007).
- <sup>30</sup> C. Himwas, M. den Hertog, Le Si Dang, E. Monroy, and R. Songmuang, *Appl. Phys. Lett.* 105, 241908 (2014).
- <sup>31</sup> M. Azadmand, T. Auzelle, J. Lähnemann, G. Gao, L. Nicolai, M. Ramsteiner, A. Trampert, O. Brandt, S. Sanguinetti, and L. Geelhaar (unpublished).
- <sup>32</sup> R. Songmuang, G. Katsaros, E. Monroy, P. Spathis, C. Bougerol, M. Mongillo, and S. De Franceschi, *Nano Lett.* 9, 3545 (2010).
- <sup>33</sup> K. Hestroffer, C. Leclere, C. Bougerol, H. Renevier, and B. Daudin, *Phys. Rev. B* 84, 245302 (2011).
- <sup>34</sup> M. I. den Hertog, F. González-Posada, R. Songmuang, J. L. Rouviere, T. Fournier, B. Fernandez, and E. Monroy, *Nano Lett.* 12, 5691 (2012).
- <sup>35</sup> G. Li, B. Mao, F. Lan, and L. Liu, *Rev. Sci. Instrum.* 83, 113701 (2012).
- <sup>36</sup> T. Jungk, A. Hoffmann, and E. Soergel, *Appl. Phys. Lett.* 89, 163507 (2006).
- <sup>37</sup> S. Hudlet, M. Saint Jean, B. Roulet, J. Berger, and C. Guthmann, *J. Appl. Phys.* 77, 3308 (1995).
- <sup>38</sup> S. Kim, D. Seol, X. Lu, M. Alexe and Y. Kim, *Sci. Rep.* 7, 41657 (2017).
- <sup>39</sup> T. Jungk, Á. Hoffmann and E. Soergel, *New J. Phys.* 10, 013019 (2008).
- <sup>40</sup> L. Jaloustre [Dissertation]
- <sup>41</sup> S. Sivaramakrishnan, P. Mardilovich, A. Mason, A. Roelofs, T. Schmitz-Kempen, and S. Tiedke, *Appl. Phys. Lett.* 103, 132904 (2013).
- <sup>42</sup> M. Stewart, I S. Lepadatu, I L. N. McCartney, I M. G. Cain, I L. Wright, I J. Crain, D. M. Newns, and G. J. Martyna, *APL Mater.* 3, 026103 (2015).
- <sup>43</sup> S. Shetty, J. I. Yang, J. Stitt, and S. Trolier-McKinstry, *J. Appl. Phys.* 118, 174104 (2015).
- <sup>44</sup> J. Hernando, J. L. Sánchez-Rojas, S. González-Castilla, E. Iborra, A. Ababneh, and U. Schmid, *J. Appl. Phys.* 104, 053502 (2008).
- <sup>45</sup> R. Herdier, D. Jenkins, E. Dogheche, D. Rèmes, and M. Sulc, *Rev. Sci. Instrum.* 77, 093905 (2006).
- <sup>46</sup> In these particular scanning measurements, the PFM were performed at 9 kHz with a slight signal amplification evidence by the frequency dependence measurements of the cantilever resonance.
- <sup>47</sup> The piezo coefficient is obtained by following linear approximation:  $d_{33}(\text{Al}_x\text{Ga}_{1-x}\text{N}) = (1-x)d_{33}(\text{GaN}) + x d_{33}(\text{GaN})$  and  $d_{33, \text{eff}} = d_{33}(\text{AlGaIn}) L_{\text{GaIn}}/L_{\text{tot}} + d_{33}(\text{GaIn}) = L_{\text{GaIn}}/L_{\text{tot}}$ , where  $L_{\text{GaIn}}$ ,  $L_{\text{AlGaIn}}$ , and  $L_{\text{tot}}$  are the length of GaN, AlGaIn and the total length of nanowire.